Observation of Chiral Behavior in Rat Tail Tendon Fascicles

Buchanan, K., Lakes, R.. S., Vanderby, R., "Chiral behavior in rat tail tendon fascicles", Journal of Biomechanics, 64, 206-211 7 Nov. (2017). Preprint version. Figures at end.

Kimberly A. Buchanan [a,b], Roderic S. Lakes [c,d], Ray Vanderby Jr. [a,b,c,*]

[a] Department of Biomedical Engineering, University of Wisconsin-Madison, Madison, WI 53706, USA
[b] Department of Orthopedics and Rehabilitation, University of Wisconsin-Madison, Madison, WI 53705, USA
[c] Materials Science Program, University of Wisconsin-Madison, Madison, WI 53706, USA
[d] Department of Engineering Physics, University of Wisconsin-Madison, Madison, WI 53706, USA
* Corresponding author:
Department of Orthopedics and Rehabilitation
University of Wisconsin-Madison
1111 Highland Ave., Room 5059
Madison, WI 53705, USA
Tel.: +1 608 263 9593
Fax: +1 608 265 9144
E-mail: vanderby@ortho.wisc.edu

Keywords: tendon, mechanics, structure, chirality, Cosserat
2515 words

Abstract

Ex vivo tendon mechanical behavior has been well described under constrained uniaxial tensile testing. During standard loading of rat tail tendon (RTT) fascicles, apparent axial twist was observed. We designed a custom testing setup, utilizing magnetic suspension, to allow unrestrained axial rotation during tensile loading. We measured and characterized the rotational behavior of single and paired RTT fascicles under cyclic loading. Mullins-type stress softening was noted across loading cycles as well as “rotational softening”. Single fascicle nonlinear stretch-twist coupling is well described by the asymptotic function $\Delta\theta = A(1 - e^{-B\varepsilon})$ in which fascicles rotated a mean $\pm$51.1° within about 1% applied axial strain. On average, paired fascicles rotated just over 10° less. Specimen cross-sectional diameter had a noticeable effect on the measured material properties, particularly effective elastic modulus. Such stretch-twist coupling and size dependence cannot be understood via classical elasticity but is predicted by Cosserat (micropolar) elasticity. The current study demonstrates RTT fascicles are chiral based on observed axial load-induced twist. Additionally, our findings support existing research that suggest a helical fascicle structure. Potential consequences of helical substructures, mechanical and biological, should be further investigated.

1. Introduction

Tendon absorbs and transfers load between muscle and bone, and its mechanical properties are dependent on its hierarchical structure. The largest substructure of tendon is the fascicle which is composed of fibers made up of fibrils. A mature fibril is very long and consists of self-assembled collagen molecules (Kadler et al., 1996; Kastelic et al., 1978; Provenzano and Vanderby, 2006; Screen et al., 2004a). This hierarchical organization has been shown to attenuate strain in the substructures, which experience smaller strains than whole tendon (Puxkandl et al., 2002; Screen et al., 2004b; Thorpe, et al., 2012). For example, fascicles only stretch 55-90% of the 4-6% in vivo whole tendon strain (Gardiner et al., 2001; Kongsgaard et al., 2011; Lochner et al., 1980; Thorpe et al., 2012). Contributing mechanisms include the sliding that occurs between adjacent fascicles (Screen et al., 2004a, 2004b; Thorpe et al., 2012).

Ex vivo mechanical testing of tendon tissue is typically performed with constrained uniaxial tensile loading to provide a reproducible estimate of the physiological system. During tensile testing of rat tail tendon (RTT) fascicles, researchers observed rotational movement of visual strain markers (Cheng and Screen, 2007; Screen, 2008). We noted similar axial twist when mechanically stretching RTT fascicles. The presence of load-induced twist would imply fascicles are chiral, meaning they lack symmetry about their rotational axis. A ubiquitous and biologically relevant example is the helix. Helical structures have been identified at multiple hierarchical levels within tendon. The collagen I molecule is a right-handed triple helix made from three left-handed polypeptide helices. Collagen molecules self-assemble into right-handed, super-twisted microfibrils, which interdigitate with neighboring microfibrils. These units, in turn, self-assemble into larger hierarchical structures (Duenwald et al., 2009; Franchi et al., 2010; Orgel et al., 2006; Ramachandran and Kartha, 1955; Silver et al., 2003). Fiber and fascicle level helical windings have been visualized as well (Jozsa et al., 1991; Kalson et al., 2012; Kannus, 2000; Khodabakhshi et al., 2013; Thorpe et al., 2013; Vidal, 2003). Additionally, computer modeling supports the theory of higher level helices (Reese et al., 2010; Zhao et al., 2016). Helical structure could contribute to stress attenuation while increasing strain, thus leading to nonlinear load uptake (Wang et al., 2016).

Tendon has been extensively characterized as a viscoelastic, nonlinear, and anisotropic material at an apparent tissue level (Kondratko et al., 2012; Lake et al., 2009; Lynch et al., 2003; Screen, 2008; Woo et al., 1993). Existing classically elastic or viscoelastic models are not capable of modeling stretch-twist coupling behavior. An alternative that permits axial strain-rotation coupling is the Cosserat, or micropolar, theory of elasticity. Cosserat theory allows for the microrotation of points in addition to the translation afforded by classical elasticity. Instead of only 2 elastic constants, Cosserat elasticity uses 6 constants for isotropic solids and 9 for directionally isotropic chiral solids that exhibit stretch-twist coupling. A notable consequence is the presence of a size effect, or size dependence, which is not predicted in classical elasticity (Lakes, 1995; Lakes, 2001; Lakes and Benedict, 1982). Cosserat mechanics has already been applied to descriptions of biological materials such as bone and actin filaments (Park and Lakes, 1986; Yamaoka and Adachi, 2010).

To our knowledge, unconstrained rotation of tendon tissue has not been quantified experimentally. Similarly, Cosserat mechanics has not been applied to tendon. The current study characterizes the rotational behavior of RTT fascicle using Cosserat mechanics as a guide. We hypothesize RTT fascicles will exhibit stretch-twist coupling and size effects, as predicted by Cosserat elasticity; we further hypothesize the effects will be nonlinear in view of known nonlinearity of axial stress-strain curves. Additionally, Mullins effect stress softening is considered in the context of possible rotational softening. Our findings may have implications for hierarchical tendon descriptions and mechanical models. Chiral behavior would also prompt investigation into the effects stretch-twist coupling have on cell signaling and mechanotransduction.

2. Methods

2.1. Specimen preparation

Fifteen (15) Wistar rats, age 2-3 months and weight 225-325g, were humanely euthanized as approved by the University of Wisconsin Institutional Animal Use and Care Committee. The tails were kept frozen at -10°C until use. Once thawed, the skin was removed to expose the left dorsal tendon. Under a dissecting microscope, fascia was carefully cut to reveal fascicles. Some fascicles were left as intact pairs of fascicles while others were further isolated to single fascicles, at least 50 mm long from the proximal end. Twenty (20) single fascicles and ten (10) paired fascicles were dissected and immediately tested, 2 specimens (SD=1) per tendon (n=15). Hydration was maintained throughout with phosphate-buffered saline (PBS).

2.2. Mechanical testing

A custom setup within a standard servo-hydraulic testing machine (MTS Bionix 858; Eden Prairie, Minnesota) was used for mechanical testing (Fig. 1). A specimen was placed into custom spring-loaded grips spaced 45.6 mm (SD=1.3) apart within a PBS bath. The lower grip was fixed to the MTS platform. The upper grip connected to a vane and a ferromagnetic rod via a nylon line. The rod was suspended 12.8 mm (SD=0.4) from a 5 N capacity magnet attached to the actuator and a 222 N load cell. Magnetic suspension allowed frictionless rotation of the specimen and attached vane. The vane was aligned in the path of an optical LED micrometer (Keyence Corp LS-7030T; Osaka, Japan) that recorded the vane's projected width. When the displacement-controlled actuator lowered towards the rod, the magnet caused an increase in tensile force on the specimen. Due to the nonlinear magnetic field and the typical strain stiffening tissue behavior, the applied tensile force was nonlinear relative to magnet displacement (Fig. 2). Specimen deformation was measured using a linear variable differential transformer (LVDT) (Measurement Specialties Inc DC-EC 250; Hampton, Virginia) positioned over the nylon line. The line, itself, was found to stretch and twist less than 0.1% strain and 1°, respectively.

With the rod suspended from the magnet, the magnetic force on the specimen served as a preload of 0.11 N (SD=0.03) which corresponded to a preload strain of 0.7% (SD=0.8). The magnet was cyclically displaced between its starting position and a peak displacement of 6.3 mm (SD=0.2) downward toward the rod. The displacement-controlled protocol followed a cosine waveform consisting of 5 cycles at 0.5 cycle/min (Fig. 2). Data, including micrometer and LVDT voltages, were acquired at 10 Hz and output to a PC with Labtech Notebook software (Laboratory Technology Corp; Fort Collins, Colorado). Micrometer voltages were correlated to projected vane widths then vane angles via a sixth-order polynomial. LVDT voltage changes were proportional to axial displacement.

2.3. Parameter calculations

Assuming an ellipsoidal geometry, specimen cross-sectional area was calculated based on major and minor midsection diameters measured prior to testing. Average diameter and radius were used for size effect analysis and shear strain calculation, respectively. Specimen axial strain (ε) was determined by dividing the LVDT-measured displacement ($\Delta\mathrm{L}$) by the preloaded, grip-to-grip specimen length (L_0): $\varepsilon = \Delta\mathrm{L}/\mathrm{L}_0$. The absolute change in vane angle was termed axial rotation with rotation direction noted by the sign: positive (+) = clockwise (CW) and negative (-) = counterclockwise (CCW). Specimen shear strain (γ) was calculated as the measured rotation ($\Delta\theta$) multiplied by the average radius ($\mathrm{r}_{\mathrm{avg}}$) and divided by the initial, preloaded length: $\gamma = \Delta\theta\, \mathrm{r}_{\mathrm{avg}}/\mathrm{L}_0$.

The loading portion of cycle 1 was isolated to evaluate the stretch-twist relationship. The asymptotic function $\Delta\theta = A(1 - e^{-B\varepsilon})$ was used to quantify the behavior between axial strain and rotation. Stress-strain ratios (σ/ε) and shear strain to axial strain ratios (γ/ε) were compared to average diameters for possible size effects. Ratios were calculated at the time point when cycle 1 peak rotation occurred. Peak stress and peak rotation within each cycle were compared for potential specimen softening behavior. Peak stress and rotation were normalized by corresponding peak strain values. Normalized stress and rotation were then normalized to cycle 1 for comparing specimens.

2.4. Statistical analysis

Mean and standard deviation were reported for all parameters. Stretch-twist curve fit coefficients and R^2 values were calculated. Linear regressions were performed on the size effect data. One-way ANOVAs with Tukey's post-hoc tests were performed to compare single and paired fascicles, and cycles. Statistical significance was defined as $p<0.05$.

2.5. Scanning electron microscopy

Single and paired fascicles were imaged with scanning electron microscopy (SEM) to observe the underlying fibrillar structure. Immediately after dissection, specimens, about 10 mm long from the proximal end, were fixed in 2.5% glutaraldehyde in PBS for 8 hr. Specimens were dehydrated in ascending ethanol concentrations up to 100% and critical point dried. Finally, specimens were sputter coated in palladium/gold and visualized using a high-resolution scanning electron microscope (Hitachi S-3200N; Tokyo, Japan).

3. Results

3.1. Stretch-twist coupling

For single fascicles, the loading portion of the first cycle revealed a non-linear relationship between applied axial strain and measured axial rotation (Fig. 3A). The fascicles rotated 51.1° on average (SD=19.9), most of which occurred within the first 1% strain after preloading. Paired fascicles exhibited less rotation with a mean 39.7° (SD=22.7), a non-significant trend (p=0.157).

Rotation was observed in both CW and CCW directions. For the 20 single fascicles tested, 10 rotated CW and 10 CCW. Of the 10 paired fascicles, 6 rotated CW and 4 CCW. Fascicles originally part of a pair did not consistently rotate in the same nor opposite direction as their counterparts when tested individually.

The stretch-twist coupling was well described by the asymptotic function $\Delta\theta = A(1 - e^{-B\varepsilon})$ (Fig. 3B). The mean calculated function coefficients |A| and B were 49.7 (SD=18.0) and 3.37 (SD=1.17), respectively. The mean goodness-of-fit R^2 value was 0.993 (SD=0.008).

3.2. Diameter size effect

Stress-strain ratio, or effective modulus, appeared to correlate to average fascicle diameter for single and paired fascicles (Fig. 4A). For single and paired fascicles, the linear regression R^2 values were 0.773 and 0.794, respectively. The mean average diameter for single fascicles was 474 μm (SD=53) and for paired fascicles was 509 μm (SD=81; p=0.175). The mean stress-strain ratio for single and paired fascicles was 785 MPa (SD=173) and 569 MPa (SD=201), respectively ($p<0.01$).

Shear strain to axial strain ratio, another representation of stretch-twist coupling, and average diameter did not correlate as strongly. R^2 values for single and paired fascicles were 0.576 and 0.013, respectively. The mean shear-to-axial strain ratio for single and paired fascicles was 0.470 (SD=0.208) and 0.380 (SD=0.202), respectively (p=0.270).

3.3. Mullins-type softening

Normalized peak stress and normalized peak rotation were calculated for each of the 5 cycles. Peak stresses and peak rotations were normalized by corresponding peak axial strains then normalized to cycle 1. Single fascicles exhibited a reduction in normalized peak stress with each subsequent cycle (Fig. 5A). Statistically significant differences were found between all cycle comparisons (p=0.003 for cycle 4 v 5, $p<0.0001$ for all others). Normalized peak stress progressively lowered between cycles for paired fascicles as well (Fig. 5B). Compared to cycle 1, there were significant reductions for cycles 3, 4, and 5 (p=0.004, 0.002, and 0.0003, respectively).

Similarly, single and paired fascicles demonstrated smaller normalized peak rotations with each subsequent cycle. For single fascicles, cycles 2, 3, 4, and 5 were significantly less than cycle 1 (cycle 2: p=0.0001, cycles 3-5: $p<0.0001$) (Fig. 5C). Additionally, cycles 4 and 5 were significantly less than cycle 2 (p=0.003 and $p<0.0001$, respectively). Paired fascicles only had significantly smaller rotations with cycles 4 and 5 when compared to cycle 1 (p=0.016 and p=0.004, respectively) (Fig. 5D).

3.4. Scanning electron microscopy

Helical organization of the fibers could explain the observed fascicle rotation. Although the fibers were not obviously angled relative to the single fascicle (Fig. 6A), calculations indicate that fiber helical angles less than one degree would account for the measured axial rotations, given the fascicle length and radius. Upon closer examination, some images showed fibers being composed of right-handed helical fibrils (Fig. 6B). No discernable differences were noted between fascicles within a pair.

4. Discussion

The custom-built testing setup allowed measurement of unconstrained axial rotation during uniaxial tensile loading. Single fascicles displayed nonlinear stretch-twist coupling that leveled off within about 1% strain after a notable mean $\pm 51.1°$ of rotation. Paired fascicle behavior was variable since some pairs unwound during testing and others did not. Paired fascicles rotated just over 10° less than single fascicles; however, the difference was not statistically significant. Interestingly, fascicles did not all rotate in the same direction which was also noted by Cheng and Screen (2007). Opposing single fascicle handedness could explain smaller paired fascicle rotations.

Based on the observed load-induced twist, we conclude RTT fascicles behave as chiral materials. As a result, current classically elastic models and viscoelastic models are insufficient to capture this behavior. Use of an alternative theory, Cosserat elasticity, accounts for the point rotations needed to predict stretch-twist coupling in chiral rods (Lakes, 1995; Lakes, 2001; Lakes and Benedict, 1982). It is worth noting that allowing fascicles to freely rotate did not have a strong effect on the mean effective modulus. The modulus of single fascicles, 785 ± 173 MPa, was comparable to moduli of just over 800 MPa determined during constrained tensile testing (LaCroix et al., 2013).

Size effects, which are not present in classically elastic solids, are seen in Cosserat solids. There was a strong average diameter size effect on effective modulus. The effect, $\sigma/\varepsilon \propto D$, extended into the larger paired fascicles. Size had a weak linear effect on shear strain to axial strain ratio, an indicator of stretch-twist coupling, for single fascicles. There was no linear correlation for paired fascicles. Relative to the single fascicles, the paired fascicle data appeared to have 3 outliers perhaps due to pairs unwinding. If the radius is sufficiently large compared to the material characteristic length scale, shear-to-axial strain ratio is inversely related to radius, provided the material contains chiral microstructures distributed uniformly over the volume. This is not the case in fascicles as seen in the SEM images. Nevertheless, fascicles exhibited large values of stretch-twist coupling at small strains: the ratio of shear-to-axial strain is comparable to that in 3D isotropic chiral lattices designed to exhibit such effects (Ha et al., 2016).

To examine how fascicles behaved across all 5 cycles, we analyzed Mullins-type softening. We observed that load imparted by the test system produced irrecoverable strain within a given cycle causing strain to creep with each cycle. Single and paired fascicles exhibited stress softening and its rotational equivalent: rotational softening. The amount of stress per unit strain and rotation per unit strain decreased with each cycle.

A structural explanation for the observed chirality was briefly probed for using SEM imaging. Some images showed right-handed helical winding of fibrils to form the fibers. Those who have looked more extensively have also identified helices at this fiber level (Franchi et al., 2010). However, these helices would not account for the chirality witnessed at a higher hierarchical level. Images were inconclusive regarding a helical organization of fibers within a fascicle. Even so, the present experiment demonstrated substantial axial rotation during tensile loading of RTT fascicles, which supports the theory of helical organization at the fascicle level.

Integration of helical structures, especially at the fiber and fascicle levels, may be pertinent to future models and descriptions. Cosserat mechanics predicts stretched chiral rods to exhibit a non-uniform Poisson-type transverse deformation. As a result, possible non-uniform hydrostatic stress would lead to hydrostatic pressure changes within fascicles. This might contribute to various aspects of cellular behavior including cell homeostasis, cell signaling, and fluid transport. Further study of the mechanical and biological consequences of chiral behavior is warranted.

Acknowledgments

Support by the National Science Foundation (Award 1432937) is gratefully acknowledged. The authors also thank Ron McCabe for his technical assistance constructing the testing setup, and Heather Hartwig Stokes and Andrew Close for their assistance with data collection.

References

Cheng, V.W.T., Screen, H.R.C., 2007. The micro-structural strain response of tendon. Journal of Materials Science 42 (21), 8957-8965.

Duenwald, S.E., Vanderby, R., Lakes, R.S., 2009. Viscoelastic relaxation and recovery of tendon. Annals of Biomedical Engineering 37 (6), 1131-1140.

Franchi, M., De Pasquale, V., Martini, D., Quaranta, M., Macciocca, M., Dionisi, A., Ottani, V., 2010. Contribution of glycosaminoglycans to the microstructural integrity of fibrillar and fiber crimps in tendons and ligaments. The Scientific World Journal 10, 1932-1940.

Gardiner, J.C., Weiss, J.A., Rosenberg, T.D., 2001. Strain in the human medial collateral ligament during valgus loading of the knee. Clinical Orthopaedics and Related Research 391, 266-274.

Ha, C.S., Plesha, M.E., Lakes, R.S., 2016. Chiral three-dimensional isotropic lattices with negative Poisson's ratio. Physica Status Solidi (B) 253 (7), 1243-1251.

Jozsa, L., Kannus, P., Balint, J.B., Reffy, A., 1991. Three-dimensional ultrastructure of human tendons. Acta Anatomica 142 (4), 306-312.

Kadler, K.E., Holmes, D.F., Trotter, J.A., Chapman, J.A., 1996. Collagen fibril formation. Biochemical Journal 316 (1), 1-11.

Kalson, N.S., Malone, P.S.C., Bradley, R.S., Withers, P.J., Lees, V.C., 2012. Fibre bundles in the human extensor carpi ulnaris tendon are arranged in a spiral. Journal of Hand Surgery 37 (6), 550-554.

Kannus, P., 2000. Structure of the tendon connective tissue. Scandinavian Journal of Medicine and Science in Sports 10 (6), 312-320.

Kastelic, J., Galeski, A., Baer, E., 1978. The multicomposite structure of tendon. Connective Tissue Research 6 (1), 11-23.

Khodabakhshi, G., Walker, D., Scutt, A., Way, L., Cowie, R.M., Hose, D.R., 2013. Measuring three-dimensional strain distribution in tendon. Journal of Microscopy 249 (3), 195-205.

Kondratko, J., Duenwald-Kuehl, S., Lakes, R., Vanderby, R., 2012. Mechanical compromise of partially lacerated flexor tendons. Journal of Biomechanical Engineering 135 (1), 011001(1)-011001(8).

Kongsgaard, M., Nielsen, C.H., Hegnsvad, S., Aagaard, P., Magnusson, S.P., 2011. Mechanical properties of the human Achilles tendon, in vivo. Clinical Biomechanics 26 (7), 772-777.

LaCroix, A.S., Duenwald-Kuehl, S.E., Brickson, S., Akins, T.L., Diffee, G., Aiken, J., Vanderby, R., Lakes, R.S., 2013. Effect of age and exercise on the viscoelastic properties of rat tail tendon. Annals of Biomedical Engineering 41 (6), 1120-1128.
Lake, S.P., Miller, K.S., Elliott, D.M., Soslowsky, L.J., 2009. Effect of fiber distribution and realignment on the nonlinear and inhomogeneous mechanical properties of human supraspinatus tendon under longitudinal tensile loading. Journal of Orthopaedic Research 27 (12), 1596-1602.
Lakes, R.S., 1995. Experimental methods for study of Cosserat elastic solids and other generalized elastic continua. In: Mühlhaus, H.B. (Ed.), Continuum models for materials with microstructure. Wiley, New York, pp. 1-22.
Lakes, R.S., 2001. Elastic and viscoelastic behavior of chiral materials. International Journal of Mechanical Sciences 43 (7), 1579-1589.
Lakes, R.S., Benedict, R.L., 1982. Noncentrosymmetry in micropolar elasticity. International Journal of Engineering Science 20 (10), 1161-1167.
Lochner, F.K., Milne, D.W., Mills, E.J., Groom, J.J., 1980. In vivo and in vitro measurement of tendon strain in the horse. American Journal of Veterinary Research 41 (12), 1929-1937.
Lynch, H.A., Johannessen, W., Wu, J.P., Jawa, A., Elliott, D.M., 2003. Effect of fiber orientation and strain rate on the nonlinear uniaxial tensile material properties of tendon. Journal of Biomechanical Engineering 125 (5), 726-731.
Orgel, J.P.R.O., Irving, T.C., Miller, A., Wess, T.J., 2006. Microfibrillar structure of type I collagen in situ. Proceedings of the National Academy of Sciences of the United States of America 103 (24), 9001-9005.
Park, H.C., Lakes, R.S., 1986. Cosserat micromechanics of human bone: strain redistribution by a hydration-sensitive constituent. Journal of Biomechanics 19 (5), 385-397.
Provenzano P.P., Vanderby, R., 2006. Collagen fibril morphology and organization: Implications for force transmission in ligament and tendon. Matrix Biology 25 (2), 71-84.
Puxkandl, R., Zizak, I., Paris, O., Keckes, J., Tesch, W., Bernstroff, S., Fratzl, P., 2002. Viscoelastic properties of collagen: synchrotron radiation investigations and structural model. Philosophical Transactions of The Royal Society B: Biological Sciences 357 (1418), 191-197.
Ramachandran, G.N., Kartha, G., 1955. Structure of collagen. Nature 176 (4482), 593-595.
Reese, S.P., Maas, S.A., Weiss, J.A., 2010. Micromechanical models of helical superstructures in ligament and tendon fibers predict large Poisson's ratios. Journal of Biomechanics 43 (7), 1394-1400.
Screen, H.R.C., 2008. Investigating load relaxation mechanics in tendon. Journal of the Mechanical Behavior of Biomedical Materials 1 (1), 51-58.
Screen, H.R.C., Bader, D.L., Lee, D.A., Shelton, J.C., 2004a. Local strain measurement within tendon. Strain 40 (4), 157-163.
Screen, H.R.C., Lee, D.A., Bader, D.L., Shelton, J.C., 2004b. An investigation into the effects of the hierarchical structure of tendon fascicles on micromechanical properties. Proceedings of the Institution of Mechanical Engineers, Part H: Journal of Engineering in Medicine 218 (2), 109-119.

Silver, F.H., Freeman, J.W., Seehra, G.P., 2003. Collagen self-assembly and the development of tendon mechanical properties. Journal of Biomechanics 36 (10), 1529-1553.
Thorpe, C.T., Klemt, C., Riley, G.P., Birch, H.L., Clegg, P.D., Screen, H.R.C., 2013. Helical sub-structures in energy-storing tendons provide a possible mechanism for efficient energy storage and return. Acta Biomaterialia 9 (8), 7948-7956.
Thorpe, C., Udeze, C.P., Birch, H.L., Clegg, P.D., Screen, H.R.C., 2012. Specialization of tendon mechanical properties results from interfascicular differences. Journal of The Royal Society Interface 9 (76), 3108-3117.
Vidal, B.C., 2003. Image analysis of tendon helical superstructure using interference and polarized light microscopy. Micron 34 (8), 423-432.
Wang, L., Cui, Y., Qin, Q., Wang, H., Wang, J., 2016. Helical fiber pull-out in biological materials. Acta Mechanica Solida Sinica 29 (3), 245-256.
Woo, S.L., Johnson, G.A., Smith, B.A., 1993. Mathematical modeling of ligaments and tendons. Journal of Biomechanical Engineering 115 (4B), 468-473.
Yamaoka, H., Adachi, T., 2010. Coupling between axial stretch and bending/twisting deformation of actin filaments caused by a mismatched centroid from the center axis. International Journal of Mechanical Sciences 52 (2), 329-333.
Zhao, Z., Li, B., Feng, X., 2016. Handedness-dependent hyperelasticity of biological soft fibers with multilayered helical structures. International Journal of Non-Linear Mechanics 81, 19-29.

Figure Captions

Figure 1. Custom setup within a servo-hydraulic test machine for measuring unconstrained axial rotation of a tissue specimen during uniaxial tensile loading. A specimen was gripped and submerged in phosphate-buffered saline. Force on the specimen-vane-rod system changed as the actuator and magnet displaced. Specimen rotation was recorded by an optical micrometer monitoring the rotating vane. Specimen axial deformation was measured by a linear variable differential transformer (LVDT).

Figure 2. Testing protocol was a displacement-controlled cosine waveform (solid black). The nonlinear magnetic field resulted in the representative, nonlinear loading waveform (interrupted blue). The actuator and magnet were lowered 6.3 mm (SD=0.2) toward the ferromagnetic rod and returned for 5 complete cycles at 0.5 cycle/min. At least 1 N of load was applied to the specimen.

Figure 3. Cycle 1 loading of single fascicles. (A) Applied percent fascicle strain and the measured degrees of rotation (+ = clockwise, - = counterclockwise) for each fascicle (n=20). (B) Representative fascicle rotation-strain curve (black closed circle) with the asymptotic curve fit $\Delta\theta = A(1 - e^{-B\varepsilon})$ (blue solid line; A=-48.7, B=5.27, R^2=0.999).

Figure 4. Effect of average single fascicle diameter (blue circle; n=20) and average paired fascicle diameter (cyan triangle; n=10) on (A) stress-strain ratio (R^2=0.773 and 0.794, respectively) and (B) shear strain to axial strain ratio (R^2=0.576 and 0.013, respectively).

Figure 5. Peak stress normalized by corresponding peak strain across 5 cycles and normalized to cycle 1: (A) for single fascicles (n=20), all cycle comparisons were different ($p<0.01$), and (B) for paired fascicles (n=10), cycles 3-5 were reduced compared to cycle 1 ($p<0.01$). Peak rotation normalized by corresponding peak strain across 5 cycles and normalized to cycle 1: (C) for single fascicles, cycles 2-5 were smaller than cycle 1 ($p<0.001$) and cycles 4-5 were smaller than cycle 2 ($p<0.01$), and (D) for paired fascicles, cycles 4-5 were smaller than cycle 1 ($p<0.05$). Error bars represent standard error. (1) = significantly different from cycle 1, (2) = significantly different from cycle 2, and so on ($p<0.05$).

Figure 6. Single fascicle surface imaged with scanning electron microscopy to visualize structural organization of (A) the fibers within a fascicle which appeared relatively linear (bar=500 μm) and (B) the fibrils within the fibers which appeared to show right-handed helical winding of the fibrils (bar=10 μm).

Figures

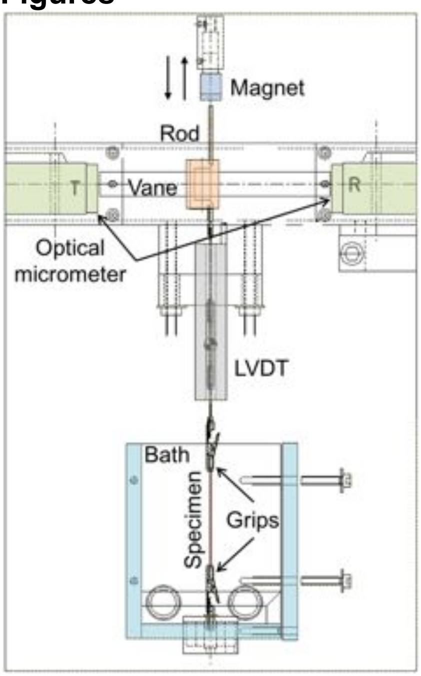

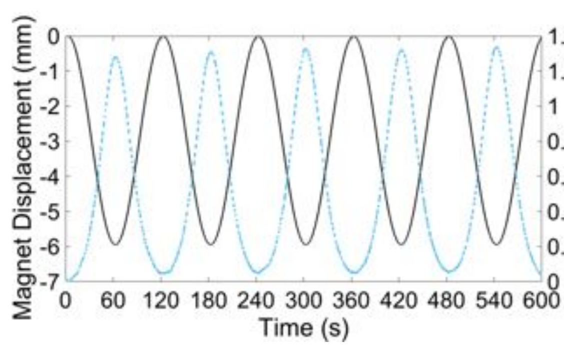

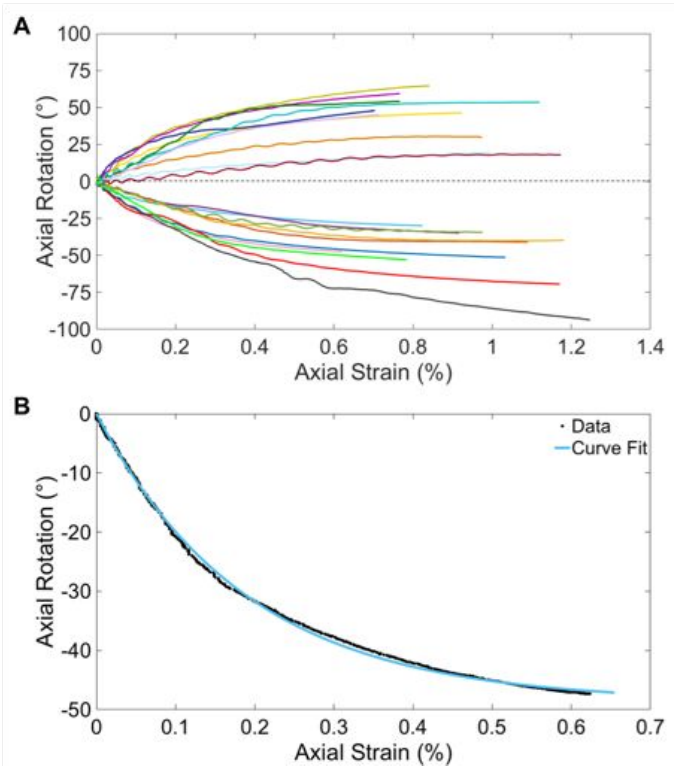
A
100
75
50
25
0
-25
-50
-75
-100
Axial Rotation (°)
0
0.2
0.4
0.6
0.8
1
1.2
1.4
Axial Strain (%)
B
0
-10
-20
-30
-40
-50
Axial Rotation (°)
· Data
Curve Fit
0
0.1
0.2
0.3
0.4
0.5
0.6
0.7
Axial Strain (%)

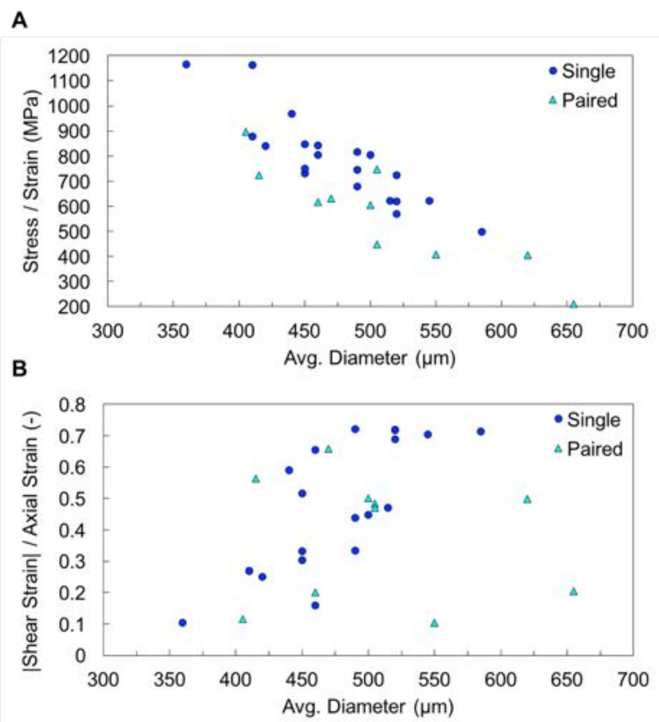
A
1200
1100
1000
900
800
700
600
500
400
300
200
Stress / Strain (MPa)
Single
Paired
300
350
400
450
500
550
600
650
700
Avg. Diameter (μm)
B
0.8
0.7
0.6
0.5
0.4
0.3
0.2
0.1
0
|Shear Strain| / Axial Strain (-)
Single
Paired
300
350
400
450
500
550
600
650
700
Avg. Diameter (μm)

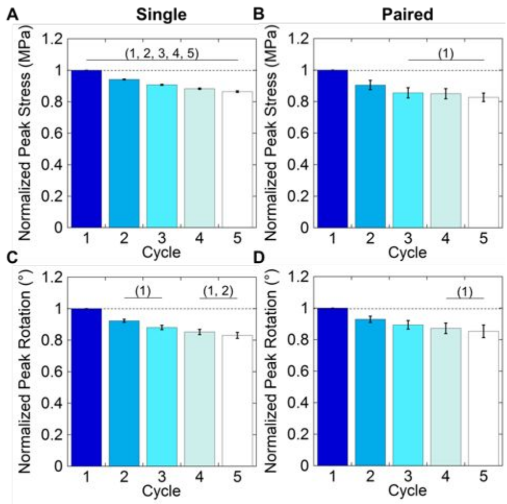
A
Single
B
Paired
(1, 2, 3, 4, 5)
(1)
Normalized Peak Stress (MPa)
Cycle
C
D
(1)
(1, 2)
(1)
Normalized Peak Rotation (°)
Cycle

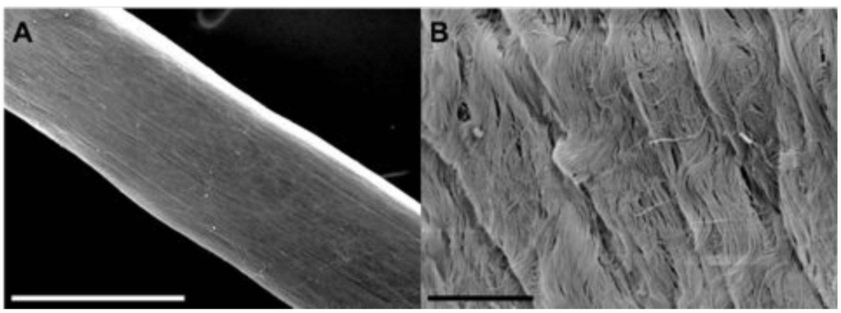
A
B